BOLETIN DE LA SOCIEDAD ESPAÑOLA DE
Cerámica y Vidrio
www.elsevier.es/bsecv

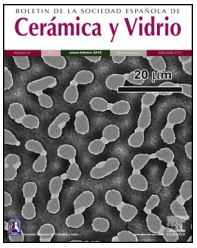

Preparation of SiC–ZrC composite powders by carbothermal reduction method and its high-temperature oxidation resistance performance

Yu Cao[a,b], *Yueming Li*[a,*], *Kai Li*[a], *Chuanming Zou*[a], *Longteng Deng*[b], *Jilin Hu*[b], *Jin Wen*[b]

[a] *China National Light Industry Key Laboratory of Functional Ceramic Materials, School of Materials Science and Engineering, Jingdezhen Ceramic University, Jingdezhen, China*
[b] *Hunan Provincial Key Laboratory of Fine Ceramics and Powder Materials, School of Materials and Environmental Engineering, Hunan University of Humanities, Science and Technology, Loudi, China*

ARTICLE INFO

Article history:
Received 10 June 2025
Accepted 10 September 2025
Available online 26 September 2025

Keywords:
Carbothermal reduction method
Silicon carbide-zirconium carbide
Composite powders
Preparation
High-temperature oxidation resistance

ABSTRACT

Ultra-high temperature ceramic materials possess irreplaceable value in extreme environments, among which SiC–ZrC multiphase ceramics have emerged as a research focus due to their exceptional high-temperature performance. The synthesis of high-quality composite powders is pivotal for the fabrication of high-performance ceramics. To address the limitations of conventional carbothermal reduction methods—including impurity contamination from organic carbon sources, inadequate reaction stability, and the paucity of research on the oxidation behavior and biphase synergistic mechanisms of SiC–ZrC composite powders—this study developed a novel controlled carbothermal reduction process using high-purity graphite as the carbon source (argon atmosphere, 1400–1600 °C). Systematic investigations were conducted to elucidate the regulatory effects of calcination temperature on the phase composition, microstructure, and elemental distribution of the powders. Additionally, high-temperature oxidation experiments under air atmosphere were performed to reveal the oxidation behavior characteristics and biphase synergistic mechanisms of the powders. The results demonstrate that high-purity SiC–ZrC composite powders with uniformly distributed elements can be successfully synthesized at 1600 °C with a 1.5-h holding time. During high-temperature oxidation, SiC exhibits significantly superior oxidation resistance compared to ZrC:ZrC initiates oxidation to form ZrO_2 as early as 800 °C, while SiC retains excellent structural stability even at 1500 °C. The two phases achieve synergistic oxidation enhancement through the formation of SiO_2–ZrO_2 composite oxide layers and $ZrSiO_4$ phases.

* *Corresponding author.*
E-mail address: lym6329@163.com (Y. Li).
https://doi.org/10.1016/j.bsecv.2025.100469

Preparación de polvos compuestos de SiC-ZrC mediante el método de reducción carbotérmica y su resistencia a la oxidación a altas temperaturas

Palabras clave:
Método de reducción carbotérmica
Carburo de silicio-carburo de circonio
Polvos compuestos
Preparación
Resistencia a la oxidación a alta temperatura

RESUMEN

Los materiales cerámicos de ultraalta temperatura presentan un valor irreemplazable en entornos extremos, entre los cuales las cerámicas multifásicas SiC-ZrC se han consolidado como foco de investigación gracias a su excepcional comportamiento a altas temperaturas. La síntesis de polvos compuestos de alta calidad es un factor crucial para la fabricación de cerámicas de alto rendimiento. A fin de abordar las limitaciones inherentes a los métodos convencionales de reducción carbotérmica —como la contaminación por impurezas derivadas de fuentes de carbono orgánico, la estabilidad insuficiente del proceso reactivo y la escasez de estudios sobre el comportamiento oxidativo y los mecanismos de sinergia bifásica de los polvos compuestos SiC-ZrC—, este trabajo ha desarrollado un novedoso proceso de reducción carbotérmica controlada basado en grafito de alta pureza como fuente de carbono (atmósfera de argón, 1400–1600 °C). Se realizaron investigaciones sistemáticas para dilucidar los efectos reguladores de la temperatura de calcinación sobre la composición de fases, la microestructura y la distribución elemental de los polvos. Asimismo, se llevaron a cabo experimentos de oxidación a alta temperatura en atmósfera de aire para revelar las características del comportamiento oxidativo y los mecanismos de sinergia bifásica de los polvos estudiados. Los resultados demuestran que es posible sintetizar con éxito polvos compuestos SiC-ZrC de alta pureza con una distribución uniforme de elementos a 1600 °C con un tiempo de mantenimiento de 1,5 horas. Durante la oxidación a alta temperatura, el SiC exhibe una resistencia a la oxidación significativamente superior a la del ZrC: mientras que el ZrC inicia su oxidación para formar ZrO_2 ya a 800 °C, el SiC mantiene una excelente estabilidad estructural incluso a 1500 °C. Ambas fases logran una mejora sinérgica en la resistencia a la oxidación mediante la formación de capas de óxido compuesto SiO_2-ZrO_2 y fases de $ZrSiO_4$.

Introduction

Ultra-high-temperature ceramic (UHTC) materials exhibit exceptional properties, such as high melting points, exceptional hardness, strong chemical stability and excellent thermal shock resistance, while maintaining robust mechanical performance and oxidation resistance at elevated temperatures [1–3]. These materials are widely utilized across diverse fields, including metallurgy, electronics, energy, and aerospace, and in applications such as cutting tools. For example, they are used as linings for metallurgical furnaces and crucibles, where their resistance to corrosion and erosion from molten metals extends equipment lifespan. In electronics, UHTCs function as heat-dissipating components for high-power devices, leveraging their high thermal conductivity and temperature resistance to efficiently manage operational heat. In cutting tool applications, they facilitate the fabrication of durable tools that retain cutting efficiency and longevity under high-speed or dry machining conditions due to their exceptional hardness and thermal stability. Additionally, in the aerospace field, UHTCs are employed in thermal protection systems for spacecraft and engine nozzles [4]. These distinctive qualities render UHTC materials indispensable for applications operating in extreme environments [5–7].

SiC–ZrC composite ceramics are formed by combining two high-melting-point carbides: SiC (melting point 2700 °C) and ZrC (melting point 3540 °C). These ceramics combine the individual advantages of each component to form a synergistically reinforced system with high strength, high toughness, and exceptional high-temperature stability and mechanical properties [8–10]. Such composites meet the stringent requirements for high-performance materials under extreme operating conditions, positioning them as promising high-temperature structural materials with broad application prospects [11,12].

The key to preparing high-performance SiC–ZrC composite ceramics lies in the synthesis of high-quality SiC–ZrC ultrafine composite powders. These powders must exhibit uniform particle distribution, controlled morphology, small particle size, and high sintering activity. The primary methods for synthesizing ultrafine SiC–ZrC composite powders include self-propagating high-temperature synthesis (SHS), carbothermal reduction [13–16], sol–gel method [17–20], liquid precursor method [21,22] and chemical vapour deposition (CVD) [23]. The SHS method prepares SiC–ZrC composite powders through the exothermic reaction of Si–Zr–C mixed powders. However, this approach suffers from poor controllability of the combustion process, significant fluctuations in product purity, and difficulties in achieving scalable indus-

trial production. The sol–gel method is limited by high raw material costs, long processing cycles, complex procedures, low production efficiency and scalability issues for industrial applications. CVD, while effective, requires substantial equipment investment and exhibits low deposition efficiency. By contrast, the carbothermal reduction method is distinguished by its low-cost raw materials, simple synthesis process, controllable reaction conditions, cost-effectiveness and suitability for large-scale production, all of which contribute to its widespread adoption in industrial chemical synthesis. Wang et al. [13] synthesized ZrC/SiBCN aerogels by using zirconium butoxide-modified polyborosilazane as a precursor through solvothermal reactions, freeze-casting, freeze-drying and pyrolysis. Subsequent pyrolysis-induced stepwise carbothermal reduction between oxygen-containing phases and free carbon resulted in the in situ formation of core–shell structured ZrC@SiC nanocrystals within an amorphous SiBCN matrix. This process effectively suppressed the crystallization and growth of SiC crystals. Liu et al. [14] prepared SiC–ZrC composite powders through microwave-assisted carbothermal reduction, using zircon and activated carbon as raw materials. Their thermodynamic analysis and investigation of reaction temperature, additive dosage (e.g., B_2O_3) and powder embedding conditions revealed that elevated temperatures and B_2O_3 addition facilitated synthesis, whereas embedding reactants in SiC powder inhibited the process. Lei et al. [15] employed a sol–gel method combined with boron/carbothermal reduction to fabricate ZrB_2–SiC–ZrC (ZSZ) composite powders with C/(B + Zr + Si) molar ratios of 1.5, 1.9 and 2.4. Systematic studies on heat treatment temperatures (1100–1600 °C) and holding times (1–2.5 h) demonstrated that under optimized conditions (C/(B + Zr + Si) = 2.4, 1500 °C, 2.5 h), the precursors were fully converted into ZSZ powders through solid-state reactions. The resulting powders exhibited a typical core–shell structure composed of ZSZ particles as the core and a low-crystallinity ZrB_2 phase forming the outer shell.

While substantial efforts have been devoted to exploring the oxidation resistance mechanisms of SiC–ZrC bulk materials and coatings, investigations into the oxidation behavior of SiC–ZrC composite powders remain critically underexplored. Owing to their high specific surface area, these powders exhibit fundamentally distinct oxidation thresholds compared to dense bulk counterparts: bulk materials demonstrate delayed oxidation due to hindered oxygen diffusion pathways, whereas powders may undergo non-equilibrium oxidation at lower temperatures (e.g., anomalous oxidation rates, unstable phase composition of oxidation products) resulting from heightened surface reactivity and enlarged oxygen-contact interfaces. Therefore, this study focuses on elucidating oxidation behavior patterns in powdered states, with particular emphasis on clarifying synergistic mechanisms between phases. This work aims to address critical knowledge gaps in powder oxidation theory and provide foundational support for understanding oxidation characteristics in multiphase ceramic precursors.

Capitalizing on the industrial promise of carbothermal reduction and persistent voids in powder oxidation research, this study pursues three primary objectives: (1) To develop a controlled carbothermal reduction process using high-purity graphite as carbon source (argon atmosphere/1400–1600 °C), eliminating impurity introduction and reaction instability associated with organic carbon sources; (2) To correlate calcination temperature with quantitative phase composition, microstructural characteristics (e.g., particle morphology, agglomeration), and size distribution; (3) To decipher biphase synergistic oxidation mechanisms via high-temperature air oxidation experiments, quantifying synergistic enhancement effects in SiC–ZrC powders to enable oxidation-resistant design paradigms for high-performance multiphase ceramics.

Experimental procedure

Graphite (C, ≥99%, Sinopharm Chemical Reagent Co., Ltd., China), zirconium dioxide (ZrO_2, ≥98.5%, Sinopharm Chemical Reagent Co., Ltd., China), and silica sol ($mSiO_2{\cdot}nH_2O$, industrial grade, 27% SiO_2 content, Changsha Water Glass Factory, Hunan, China) were selected as raw materials. The stoichiometric ratio of SiC to ZrC in the final product was set at 7:3 (molar ratio). According to the predetermined formulation, graphite, silica sol, and ZrO_2 were weighed sequentially and placed in a ball mill jar. Zirconia milling balls and an ethanol–water solution (a small amount of ethanol was added to disperse graphite effectively) were introduced. The mass ratio among raw materials, milling balls, and liquid phase was set to 1:2:2, the jar was mounted on a planetary ball mill and mixed at 400 rpm for 4 h. The resulting slurry was transferred to a 100 °C electric blast drying oven. The dried precursor powder was further refined using an agate mortar, and a portion of the processed powder was loaded into a ceramic boat, which was placed in a high-temperature tubular furnace. In argon atmosphere, the temperatures were set at 1400 °C, 1450 °C, 1500 °C, 1550 °C, and 1600 °C for 1.5 h (heating rate: ~10 °C/min) to synthesize SiC–ZrC composite powders. After cooling to room temperature in the furnace, the powder synthesized at 1600 °C was weighed and placed in a corundum crucible. Oxidation tests were conducted in a high-temperature box furnace in air atmosphere at 800 °C, 1000 °C, 1200 °C, and 1500 °C for 30 min each to evaluate its high-temperature oxidation resistance.

The mass of the SiC–ZrC composite powders before and after high-temperature calcination was measured using an electronic analytical balance to calculate the mass loss rate during synthesis and assess the extent of the synthesis reaction. Phase composition analysis was performed on powders synthesized at different calcination temperatures under an argon atmosphere, as well as on oxidation-treated products, using a Y-2000A X-ray diffractometer. Microstructural characterization of the powders was conducted with a Zeiss Sigma 500 scanning electron microscope coupled with an energy-dispersive X-ray spectroscopy (EDX) system to analyze localized elemental composition and distribution, and further elucidate the material's chemical homogeneity.

Results and discussion

Fig. 1 presents the X-ray diffraction (XRD) pattern of the dried precursor mixed powder in a Si/Zr molar ratio of 7:3. Only the characteristic diffraction peaks of C and ZrO_2 were observed in

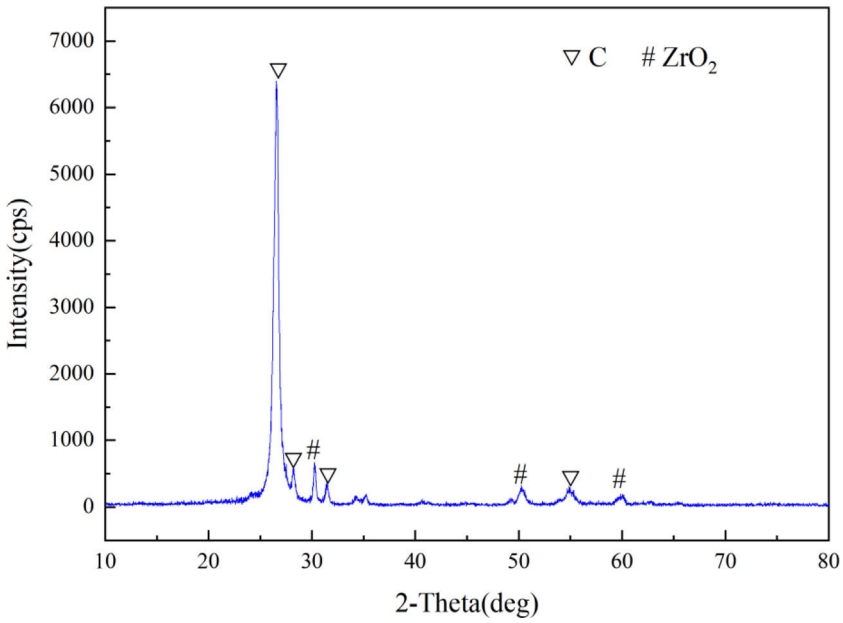

Fig. 1 – XRD pattern of the dried precursor mixed powder with a Si/Zr molar ratio of 7:3.

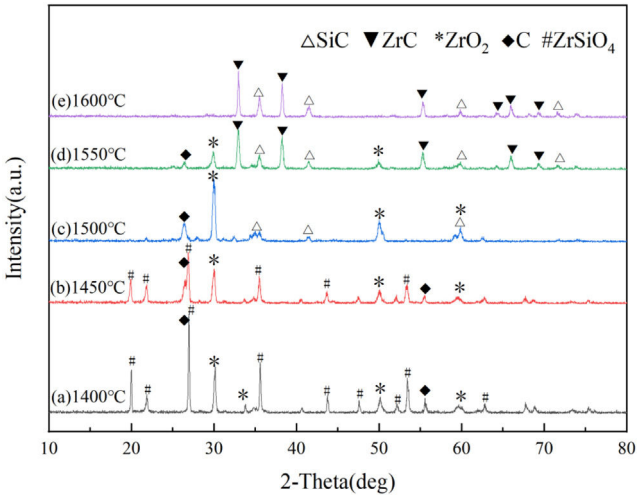

Fig. 2 – XRD patterns of powder samples synthesized under argon atmosphere at various calcination temperatures and held for 1.5 h.

the precursor, and no SiO_2 peaks were observed. The absence of SiO_2 diffraction signals is likely attributed to its amorphous state in the mixture under these conditions, which is consistent with the findings reported in [24].

Fig. 2 presents the XRD patterns of powder samples synthesized under an argon atmosphere at calcination temperatures of 1400 °C, 1450 °C, 1500 °C, 1550 °C, and 1600 °C with a holding time of 1.5 h. Calcination temperature plays a decisive role in determining the phase composition of the synthesized powders. At 1400 °C, the XRD pattern exhibits the characteristic peaks of ZrO_2 and C and diffraction peaks corresponding to the intermediate product $ZrSiO_4$. This result indicates that a solid-state reaction between ZrO_2 and SiO_2 occurred in the mixed powder under these conditions. As the temperature increases to 1450 °C, the intensity of $ZrSiO_4$ peaks diminishes considerably, suggesting the onset of its decomposition. Upon further heating to 1500 °C, the $ZrSiO_4$ peaks disappear completely, whereas weak SiC diffraction peaks emerge alongside residual ZrO_2 and C peaks, which demonstrates the initiation of carbothermal reduction between SiO_2 and C. At 1550 °C, distinct SiC and ZrC peaks dominate the XRD pattern, though weak ZrO_2 and C peaks persist, indicating an incomplete reaction. Finally, at 1600 °C, only sharp SiC and ZrC diffraction peaks were observed, confirming a nearly complete carbothermal reduction and the successful synthesis of high-purity SiC–ZrC composite powders.

During the carbothermal reduction synthesis of SiC–ZrC composite powders, solid-state reactions between carbon (from graphite) and SiO_2/ZrO_2 generated gaseous products, such as CO, which escaped from the tubular furnace with the argon flow. The measured mass loss rate of the powder samples can be calculated using the formula:

$$\text{Mass loss rate (\%)} = \frac{M1 - M2}{M1} \times 100\%, \quad (1)$$

where M_1 and M_2 represent the sample mass before and after calcination, respectively. The relative mass loss rate is then determined by:

$$\text{Relative mass loss rate (\%)} = \frac{\text{Measured mass loss rate}}{\text{Theoretical mass loss rate}} \times 100\%. \quad (2)$$

This parameter provides critical insights into the extent of reaction completion given that deviations from theoretical values reflect unreacted residues or incomplete gas evolution.

Table 1 summarizes the mass loss rate data during the synthesis of SiC–ZrC composite powders in an argon atmosphere at varying calcination temperatures. As shown in Table 1,

Table 1 – Mass loss rate during the synthesis of SiC–ZrC composite powders under an argon atmosphere at various calcination temperatures.

No.	Calcination temperature (°C)	Holding time (h)	Measured mass loss rate (%)	Theoretical mass loss rate (%)	Relative mass loss rate (%)
1#	1400	1.5	37	49	77
2#	1450	1.5	412	49	85
3#	1500	1.5	45	49	93
4#	1550	1.5	50	49	102
5#	1600	1.5	53	49	108

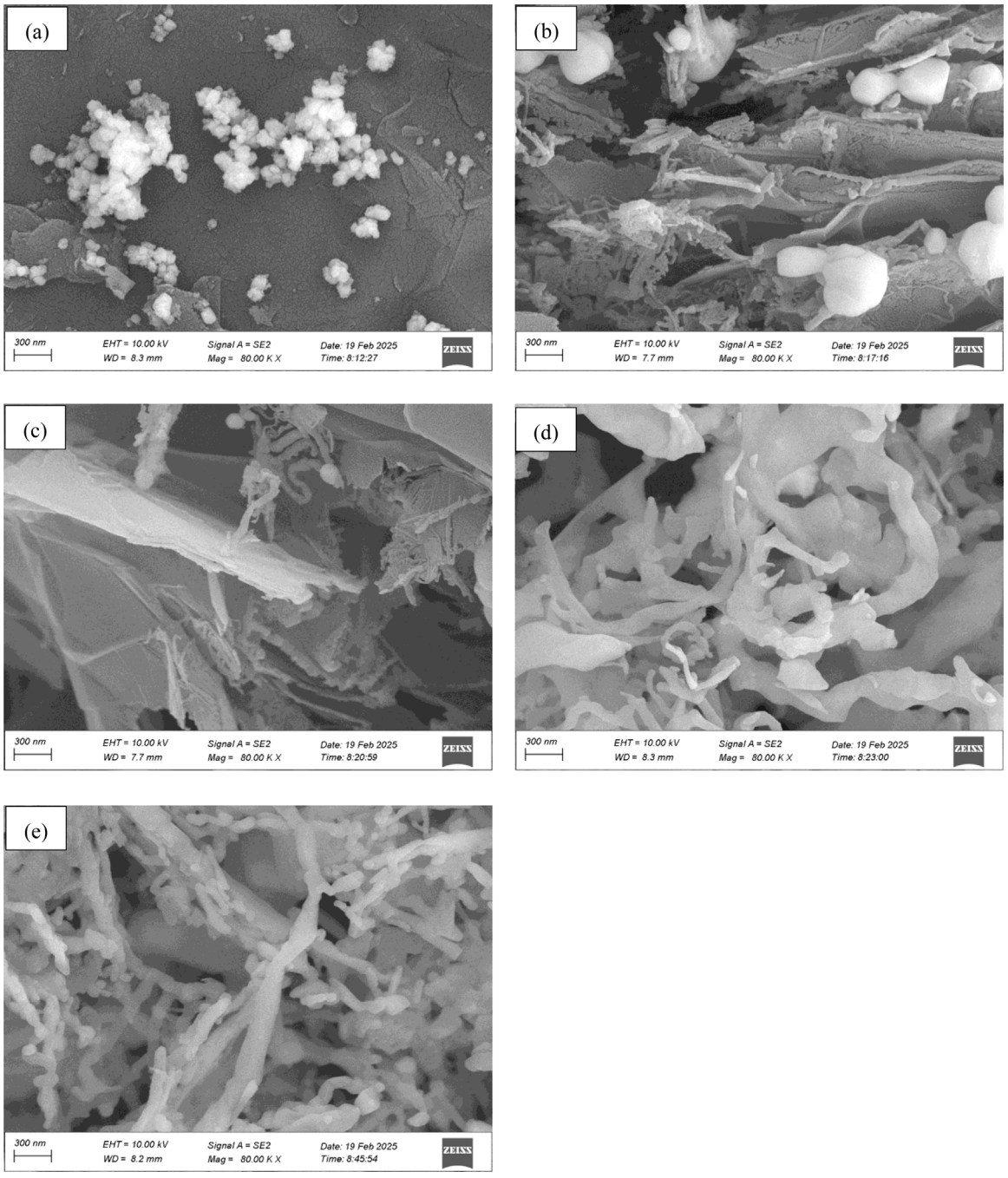

Fig. 3 – SEM micrographs of the precursor mixed powder and the powder samples synthesized in an argon-protected atmosphere at distinct temperatures with a 1.5 h isothermal hold: (a)100 °C; (b)1450 °C; (c)1500 °C; (d)1550 °C; (e)1600 °C.

the relative mass loss rate of the powder samples increases with calcination temperature. At 1400 °C, the relative mass loss rate is 77%, which increases to 93% at 1500 °C. Upon further heating to 1550 °C, the rate exceeds the theoretical mass loss rate (100%), reaching 102%, and peaking at 108% at 1600 °C. Combined with XRD analysis, these results confirm that the carbothermal reduction approaches completion when the temperature is maintained at 1600 °C for 1.5 h, enabling the synthesis of high-purity SiC–ZrC composite powders.

Under synthesis conditions maintained at 1550 °C and 1600 °C for 1.5 h, the relative mass loss rates of the powder samples (102% and 108%, respectively) exceeded the theoretical value (100%). This discrepancy primarily arises from the two-step reaction mechanism between C and SiO_2 at elevated temperatures [25–27]: The gaseous SiO intermediate forms initially and is converted into SiC. During synthesis, some of the SiO escapes the system alongside CO through the argon flow, resulting in a gaseous product loss greater than the theoretically predicted loss.

Fig. 3 displays scanning electron microscopy (SEM) micrographs of the precursor mixed powder and the powder samples synthesized in an argon-protected atmosphere. Each was calcined at distinct temperatures with a 1.5 h isothermal hold. As shown in Fig. 3a, the dried precursor exhibits diverse particle morphology, including quasi-spherical, irregularly shaped, and partially agglomerated particles. As for the sample calcined at 1450 °C (Fig. 3b), the microstructure predominantly consists of irregular, flaky and rod-like particles with interparticle aggregation and minor quasi-spherical particles. As further confirmed by XRD analysis, these particles comprise residual ZrO_2, C, and the intermediate product $ZrSiO_4$. Additionally, fine flocculent structures (Fig. 3b) are hypothesized to consist primarily of C and ZrO_2 phases derived from $ZrSiO_4$ decomposition [28]. When the temperature increases to 1500 °C (Fig. 3c), particle morphology shifts markedly to flaky and rod-like structures, and quasi-spherical particles are no longer detectable. At 1550 °C (Fig. 3d), the microstructure diverges considerably. It is composed of sparse

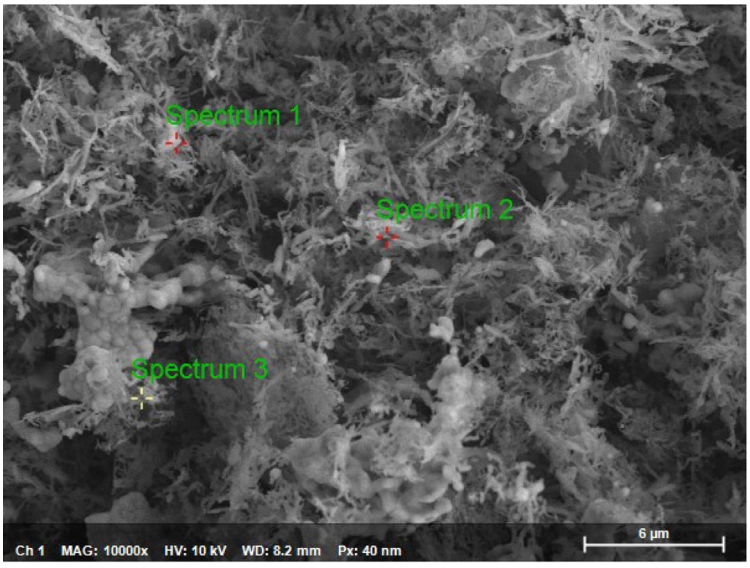

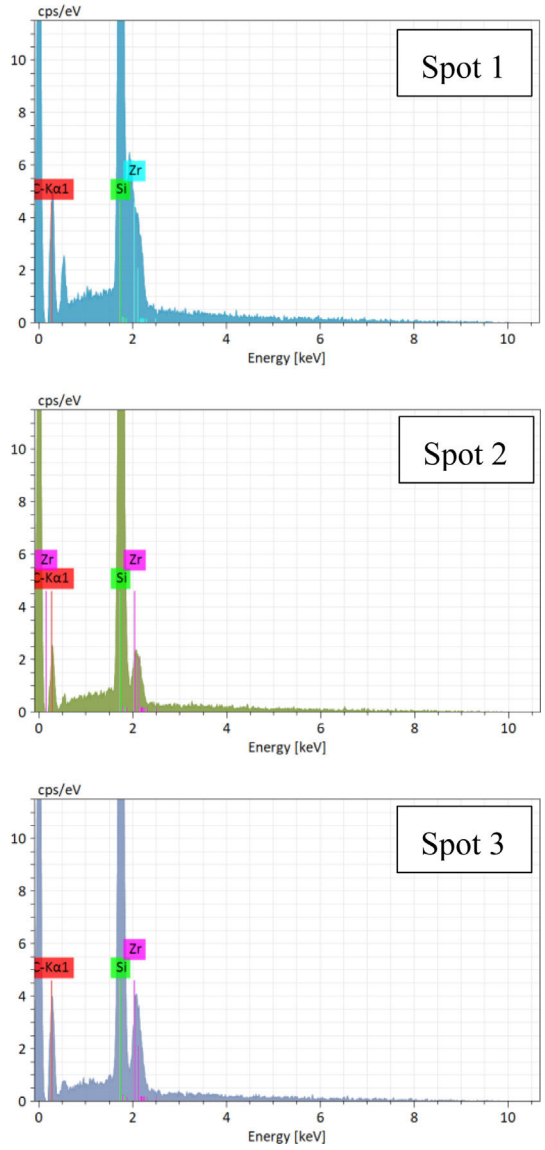

Points	w/%		
	C	Si	Zr
1	39	44	17
2	27	63	10
3	35	50	15

Fig. 4 – Point-EDX images of the micro-area of the powder sample calcined at 1600 °C for 1.5 h.

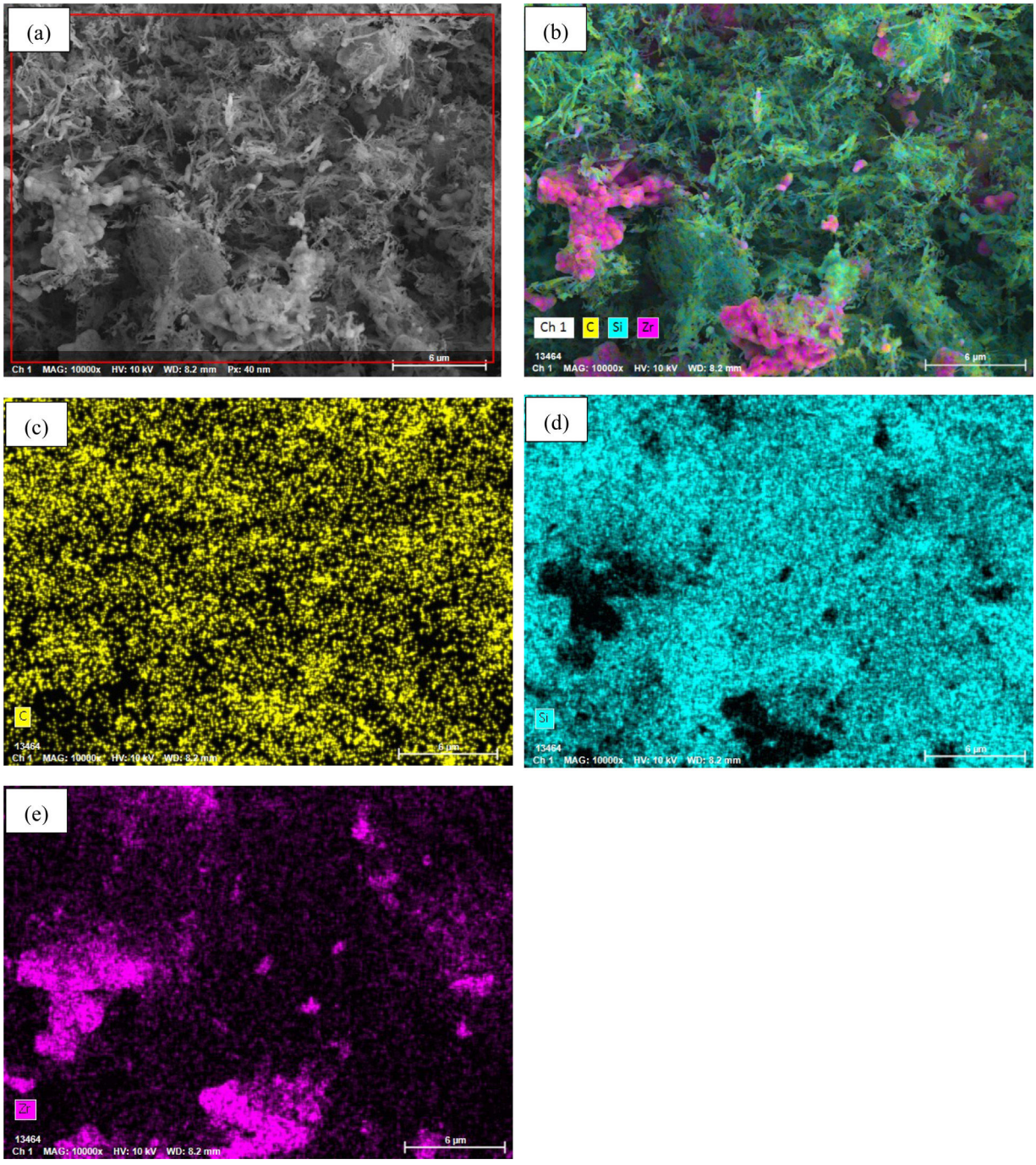

Fig. 5 – Mapping-EDX images of the micro-area of the powder sample calcined at 1600 °C for 1.5 h.

quasi-spherical and flaky particles, while abundant rod-like and whisker-shaped structures (diameters ~100 nm) emerge, forming entangled networks. In the 1600 °C sample (Fig. 3e), whisker- and rod-like structures further proliferate. XRD analysis confirms these particles as SiC and ZrC crystals, indicating the progression of carbothermal reduction with increasing temperature, ultimately yielding the target SiC–ZrC composite powders.

Figs. 4 and 5 present the EDX results of the powder synthesized at 1600 °C for 1.5 h. The powder is analyzed to accurately characterize its microstructural and chemical characteristics. Using point analysis mode (P-EDX) and elemental mapping mode (EDX mapping), quantitative elemental composition and spatial distribution patterns within the powder microregions were systematically investigated. The P-EDX spectra (Fig. 4) reveal the dominance of C, Si, and Zr. Their atomic ratios were precisely quantified. Meanwhile, the EDX mapping results (Fig. 5) visually demonstrate the homogeneous dispersion of C, Si, and Zr across the analyzed area, and no discernible elemental segregation was detected on the microscale. This uniform elemental distribution aligns with the phase composition identified through XRD analysis and

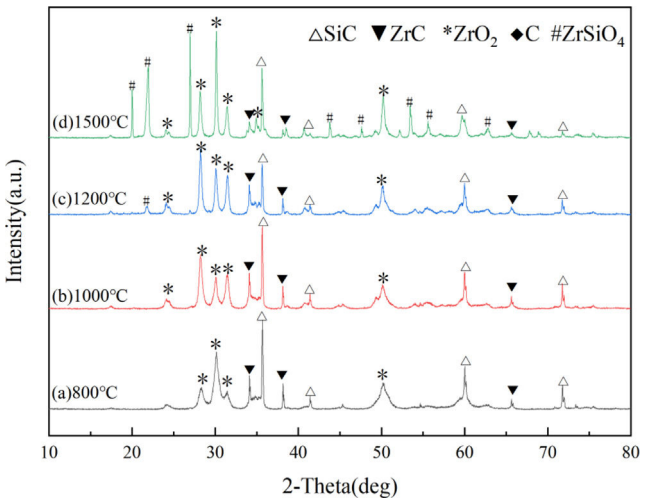

Fig. 6 – XRD patterns of SiC–ZrC composite powder oxidized at varied temperatures for 30 min.

the morphological features observed through SEM. Collectively, these multimodal characterization results confirm the successful synthesis of ultrafine SiC–ZrC composite powders under the specified experimental conditions.

Fig. 6 displays the XRD patterns of SiC–ZrC composite powders after oxidation at 800 °C, 1000 °C, 1200 °C, and 1500 °C. As shown in Fig. 6, the sample oxidized at 800 °C for 30 min exhibits the characteristic diffraction peaks of SiC and ZrC, with additional distinct ZrO_2 peaks, which indicate the partial oxidation of ZrC to ZrO_2 at this temperature. When the oxidation temperature increases to 1000 °C, the XRD pattern remains qualitatively similar, although the ZrO_2 peak intensity shows slight enhancement, suggesting the progressive intensification of ZrC oxidation with increasing temperature. A phase evolution occurs at 1200 °C. The diffraction intensities of SiC and ZrC markedly decrease, whereas the ZrO_2 peaks intensify substantially. Notably, weak $ZrSiO_4$ diffraction peaks emerge, implying the oxidation of trace SiC into SiO_2, followed by solid-state reaction between SiO_2 and ZrO_2 to form $ZrSiO_4$. At 1500 °C, while SiC maintains strong diffraction intensity, ZrC peaks further diminish. Concurrently, ZrO_2 and $ZrSiO_4$ peaks exhibit continued enhancement. This progression of phase transformations demonstrates the superior oxidation resistance of SiC compared with ZrC. Even under extreme 1500 °C oxidative conditions, SiC retains structural stability and oxidation resistance, while ZrC undergoes progressive degradation. Potential chemical reactions during air oxidation of the composite powders are summarized in Table 2.

Table 2 – Possible chemical reactions during the oxidation process of SiC–ZrC composite powder in an air atmosphere [29–32].

No.	Reaction equation
(1)	$ZrC(s) + 2O_2(g) = ZrO_2(s) + CO_2(g)$
(2)	$2ZrC(s) + 3O_2(g) = 2ZrO_2(s) + 2CO(g)$
(3)	$2SiC(s) + 3O_2(g) = 2SiO_2(l) + 2CO(g)$
(4)	$SiC(s) + 2O_2(g) = SiO_2(l) + CO_2(g)$
(5)	$2CO(g) + O_2(g) = 2CO_2(g)$
(6)	$SiO_2(l) = SiO_2(g)$
(7)	$ZrO_2(s) + SiO_2(s) = ZrSiO_4(s)$

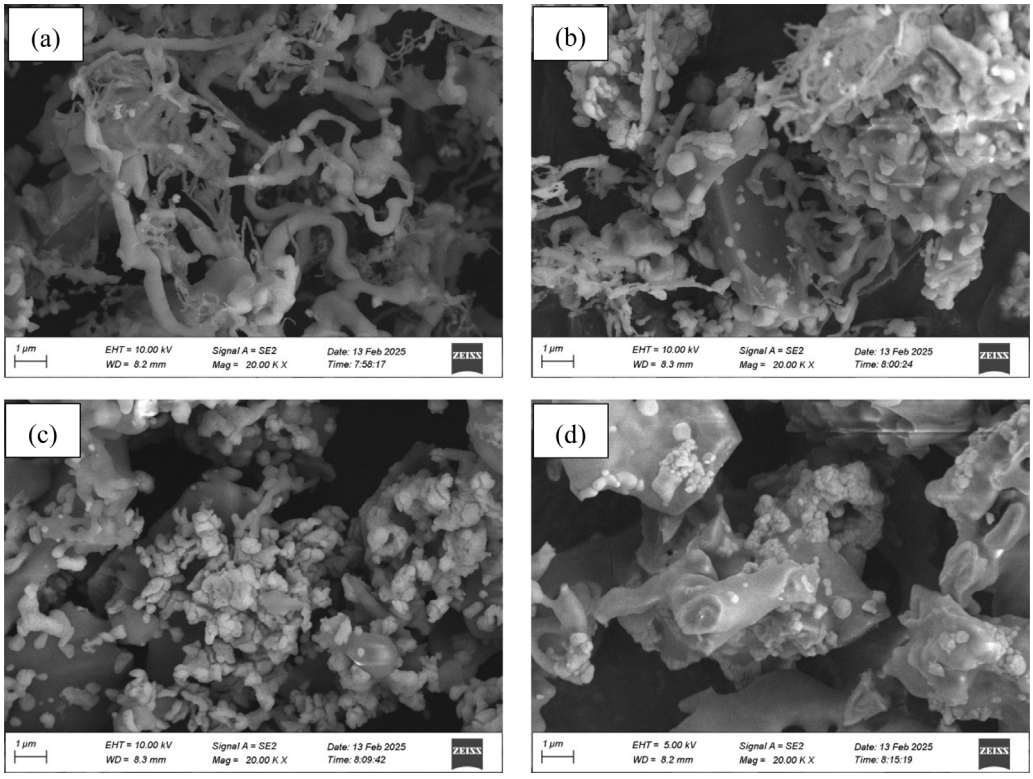

Fig. 7 – SEM micrographs of SiC–ZrC composite powder oxidized at varied temperatures for 30 min: (a)800 °C; (b)1000 °C; (c)1200 °C; (d)1500 °C.

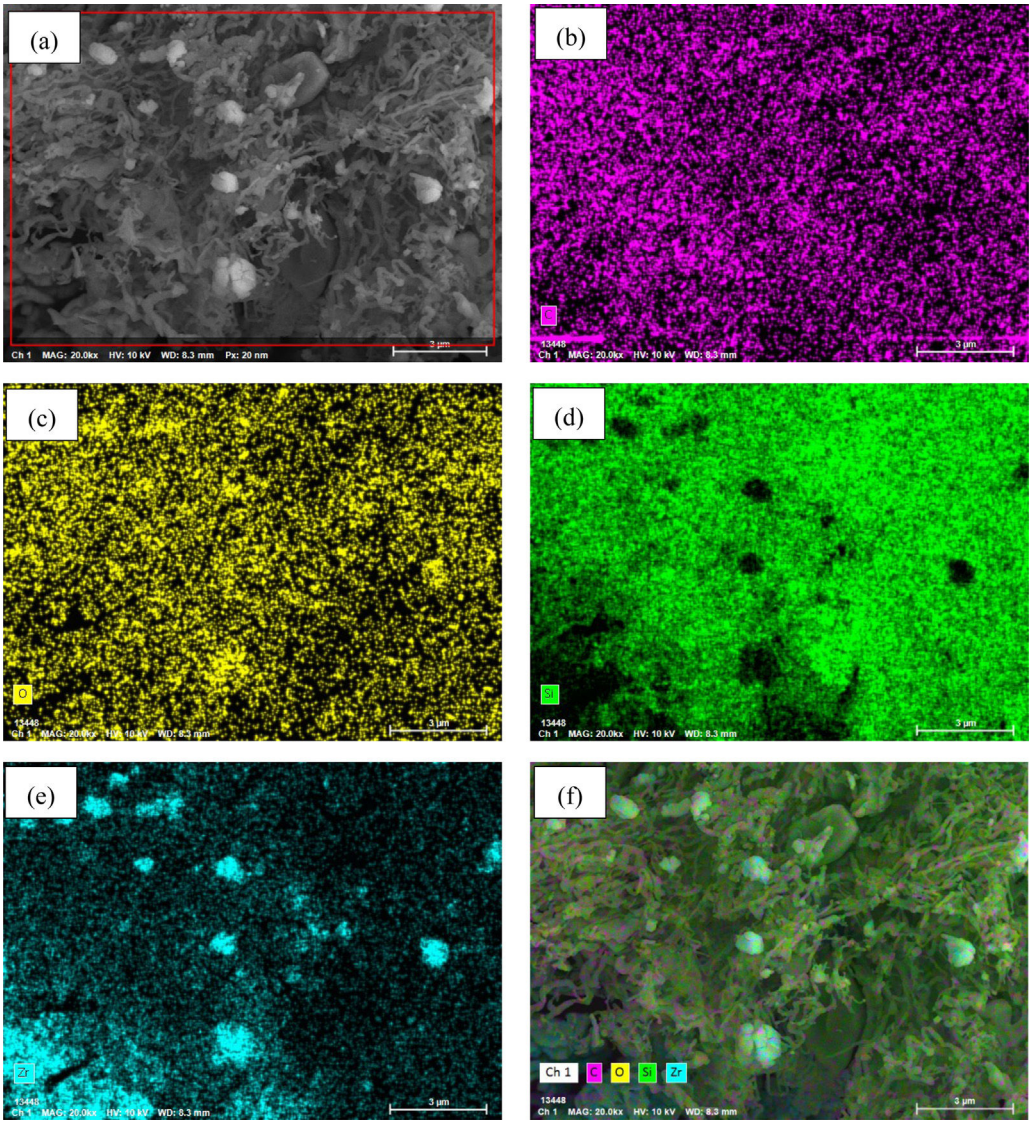

Fig. 8 – Mapping-EDX images of SiC–ZrC composite powder after oxidation at 1000 °C for 30 min.

Fig. 7 presents the SEM characterization of SiC–ZrC composite powders after 30 min of oxidation at varying temperatures. At 800 °C (Fig. 7a), the oxidized microstructure predominantly consists of rod-like structures and whisker-like phases, and entangled particles exhibit intricate interlocking configurations. As oxidation temperature increases to 1000 °C (Fig. 7b), a marked reduction in whisker content is observed, concurrent with the emergence of irregularly shaped particles that establish a diversified microstructural architecture. When the temperature reaches 1200 °C (Fig. 7c), the whisker phase completely disappears and is replaced by a heterogeneous mixture of quasi-spherical, short rod-like, and irregularly faceted particles. As the temperature further increases to 1500 °C (Fig. 7d), the powder exhibits pronounced sintering behavior characterized by substantial particle coarsening and intergranular bonding that generates agglomerated clusters.

Figs. 8 and 9 display the elemental mapping micrographs of SiC–ZrC composite powders after 30 min of oxidation at 1000 °C and 1500 °C. Both samples exhibit detectable concentrations of carbon (C), oxygen (O), silicon (Si), and zirconium (Zr), which confirm the partial oxidation of ZrC into ZrO_2 at temperatures exceeding 1000 °C. Comparative analysis of the C-distribution maps (Figs. 8b and 9b) reveals a marked reduction in carbon content within the 1500 °C specimen. This observation indicates progressive oxidation behavior: At 1000 °C, mild oxidation predominates, whereas intensified oxidation reactions are dominant at 1500 °C. The EDX findings demonstrate analytical consistency with prior XRD phase identification and SEM morphological observations, all of which validate the temperature-dependent oxidation mechanisms in the composite system.

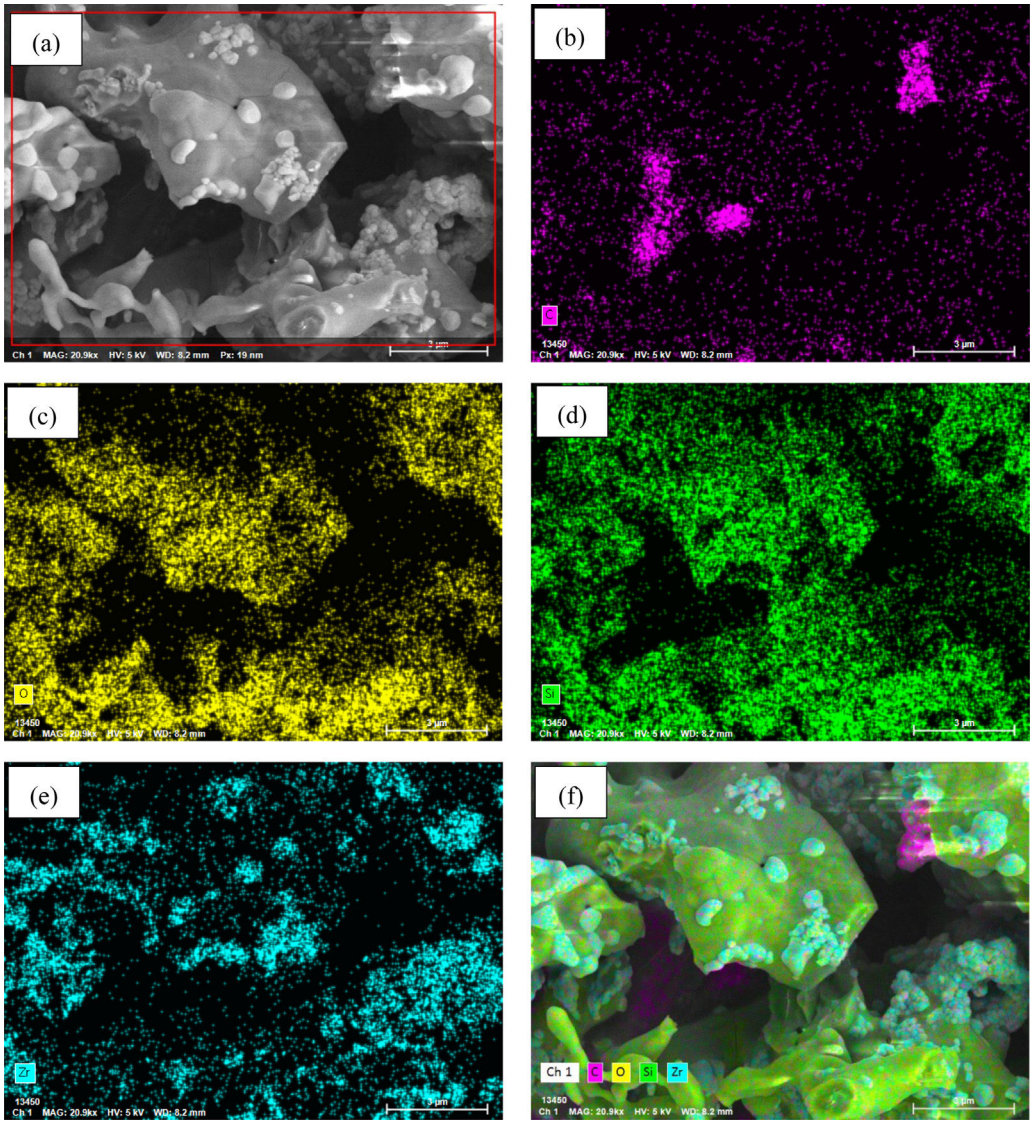

Fig. 9 – Mapping-EDX images of SiC–ZrC composite powder after oxidation at 1500 °C for 30 min.

Conclusion

In this study, efficient synthesis of SiC–ZrC composite powders was successfully achieved by developing a controlled carbothermal reduction process based on high-purity graphite as the carbon source. The research clarified the decisive role of calcination temperature in powder synthesis: as the temperature increased from 1400 °C to 1600 °C, the intermediate product $ZrSiO_4$ gradually decomposed, and the carbothermal reduction reaction progressively advanced. When the temperature reached 1600 °C with a 1.5-h holding time, the reaction was nearly complete, yielding composite powders with high purity and uniform distribution of C, Si, and Zr elements. Analysis of relative mass loss rate further confirmed that the volatilization of gaseous SiO products at high temperatures is the key factor causing the mass loss to exceed the theoretical value, providing a quantitative basis for process optimization. Meanwhile, this study systematically revealed the high-temperature oxidation behavioral patterns of SiC–ZrC composite powders, filling the research gap in the differences in oxidation mechanisms between powders and bulk materials. Oxidation experiments showed that ZrC begins to oxidize to form ZrO_2 at 800 °C, while SiC maintains relatively high structural stability even at 1500 °C. As the temperature increased from 800 °C to 1500 °C, the oxidation products gradually evolved from ZrO_2 to ZrO_2–$ZrSiO_4$ composite phases. The composite oxide layer formed by the solid-state reaction between SiO_2 and ZrO_2 constitutes the core mechanism for achieving synergistic oxidation resistance.

Funding

This research was supported by the National Natural Science Foundation of China (Grant No. 52032011), the Natural Science Foundation of Hunan Province, China (Grant No. 2025JJ70346), and Scientific Research Project of the Education Department of Hunan Province, China (Grant No. 23C0387).

Conflict of interest

No potential conflict of interest was reported by the author(s).

REFERENCES

[1] K. Ramachandran, C.J. Bear, D.D. Jayaseelan, Oxide-based ceramic matrix composites for high-temperature environments: a review, Adv. Eng. Mater. 27 (7) (2025) 2402000, http://dx.doi.org/10.1002/ADEM.202402000.

[2] R. Hassan, G.W. Fahrenholtz, K. Balani, et al., SiC addition to a dual phase high entropy ultra-high temperature ceramic, Ceram. Int. 50 (24PC) (2024) 55650–55657, http://dx.doi.org/10.1016/J.CERAMINT.2024.10.430.

[3] Y. Li, Y. Du, X. Pei, et al., High-temperature tribological behavior and mechanisms of a high entropy carbide ceramic, J. Eur. Ceram. Soc. 45 (6) (2025), http://dx.doi.org/10.1016/J.JEURCERAMSOC.2024.117170, 117170.

[4] F. Zhou, Z. Tian, B. Li, Research progress on carbide ultra-high temperature ceramic anti-ablation coatings for thermal protection system, J. Inorgan. Mater. 40 (1) (2025) 1–16.

[5] T.L. Nordström, G.O. Diaz, L. Gale, et al., Detailed study of interphase degradation in SiC/BN/SiC ceramic matrix composites after elevated temperature tensile testing, J. Eur. Ceram. Soc. 45 (4) (2025) 117039.

[6] F. Cai, D. Ni, S. Dong, Research progress of high-entropy carbide ultra-high temperature ceramics, J. Inorgan. Mater. 39 (6) (2024) 591–608, http://dx.doi.org/10.15541/jim20230562.

[7] S. Weng, Z. Deng, Z. Huang, et al., Ablation behavior and high temperature ceramization mechanism of TiB2-B4C-ZrC modified carbon fiber/boron phenolic resin composites, Ceram. Int. 50 (22PB) (2024) 46173–46186, http://dx.doi.org/10.1016/J.CERAMINT.2024.08.460.

[8] C. Xu, C. Jia, Z. Peng, et al., High-temperature properties and microstructure evolution of C/C-ZrC-SiC composites fabricated by reactive melt infiltration, J. Eur. Ceram. Soc. 45 (10) (2025) 117288, http://dx.doi.org/10.1016/J.JEURCERAMSOC.2025.117288.

[9] J. Hou, J. Zhang, S. Kou, et al., Optimizing and ablation behavior of ZrC-SiC coating prepared by a coupling process, Mater. Charact. 221 (2025) 114787, http://dx.doi.org/10.1016/J.MATCHAR.2025.114787.

[10] R. Malik, H.S. Jang, Y. Kim, et al., Mechanical properties of silicon carbide-in situ zirconium carbonitride composites, Int. J. Appl. Ceram. Technol. 16 (4) (2019) 1304–1313, http://dx.doi.org/10.1111/ijac.13213.

[11] B. Li, Y. Chen, S. Wang, Preparation and ablation performance of (ZrC/SiC)35 multilayer alternating coating with sub-micro sublayers thickness, Ceram. Int. 51 (5) (2025) 6587–6598, http://dx.doi.org/10.1016/J.CERAMINT.2024.12.103.

[12] J. Lin, Y. Chen, Q. Wang, et al., Formation mechanism of ZrC-SiC joint prepared by pulsed-current assisted diffusion bonding, Ceram. Int. 51 (3) (2025) 2996–3007, http://dx.doi.org/10.1016/J.CERAMINT.2024.11.276.

[13] H. Wang, Z. Hu, D. Su, Construction of ZrC@SiC shell-core structure in SiBCN aerogel for enhanced thermal stability and thermal insulation, Chem. Eng. J. 499 (2024) 156158, http://dx.doi.org/10.1016/J.CEJ.2024.156158.

[14] J. Liu, S. Du, X. Deng, et al., Preparation of ZrC-SiC composite powders by microwave carbothermal reduction of $ZrSiO_4$, Rare Met. Mater. Eng. 44 (S1) (2015) 217–221.

[15] Z. Lei, L. Zhanjun, Z. Hongchao, et al., Synthesis and formation mechanism of ZrC–SiC–TiC ceramic powders with high-sinterability via sol–gel process and carbothermal reduction, Ceram. Int. 50 (2PA) (2024) 2825–2835, http://dx.doi.org/10.1016/J.CERAMINT.2023.11.004.

[16] Y. Cao, R. Deng, J. Hu, et al., Synthesis and mechanism of SiC–ZrC composite powders by carbothermal reduction method, Ceram.-Silik. 66 (4) (2022) 489–497, http://dx.doi.org/10.13168/cs.2022.0045.

[17] Z. Zhou, B. Chen, C. Tao, et al., Synthesis of ZrB_2–SiC–ZrC composite powders with core-shell structure via sol–gel molecular modulation, Ceram. Int. 50 (22PC) (2024) 48391–48406, http://dx.doi.org/10.1016/J.CERAMINT.2024.09.188.

[18] C. Zeng, K. Tong, M. Zhang, et al., The effect of sol–gel process on the microstructure and particle size of ZrC-SiC composite powders, Ceram. Int. 46 (4) (2020) 5244–5251, http://dx.doi.org/10.1016/j.ceramint.2019.10.273.

[19] M. Liang, F. Li, X. Ma, et al., Syntheses of ZrC-SiC nanopowder via sol–gel method, Ceram. Int. 42 (1) (2016) 1345–1351, http://dx.doi.org/10.1016/j.ceramint.2015.09.073.

[20] Z. Lei, F. Cunqian, L. Xiao, et al., Effect of $MgCl_2$ addition on the preparation of ZrC–SiC composite particles by sol–gel, Ceram. Int. 48 (2) (2022) 2522–2532, http://dx.doi.org/10.1016/J.CERAMINT.2021.10.034.

[21] X. Lian, W. Long, J. Xu, et al., Synthesis of ZrC–SiC nano-composite powders via liquid precursor conversion and sol–gel method, Bull. Chin. Ceram. Soc. 37 (1) (2018) 195–199, http://dx.doi.org/10.16552/j.cnki.issn.1001-1625.2018.01.031.

[22] Y. Tian, Z. Feng, J. Hu, et al., One-pot synthesis precursor of SiC–ZrC composite ceramic precursor and its properties, Aerospace Mater. Technol. 50 (4) (2020) 35–38, http://dx.doi.org/10.12044/j.issn.1007-2330.2020.04.007.

[23] Q. He, H. Li, C. Wang, et al., Microstructure and ablation property of C/C-ZrC-SiC composites fabricated by chemical liquid-vapor deposition combined with precursor infiltration and pyrolysis, Ceram. Int. 45 (3) (2019) 3767–3781, http://dx.doi.org/10.1016/j.ceramint.2018.11.045.

[24] J. Hu, C. Hu, W. Guo, et al., Synthesis of SiC–TiC composite powders using glucose as carbon source, J. Synthetic Cryst. 46 (2017) 311–315, http://dx.doi.org/10.16553/j.cnki.issn1000-985x.2017.02.019.

[25] V. Raman, G. Bhatia, S. Bhardwaj, et al., Synthesis of silicon carbide nanofibers by sol–gel and polymer blend techniques, J. Mater. Sci. 40 (6) (2005) 1521–1527, http://dx.doi.org/10.1007/s10853-005-0596-9.

[26] N.K. Sharma, W.S. Williams, A. Zangvil, Formation and structure of silicon carbide whiskers from rice hulls, J. Am. Ceram. Soc. 67 (11) (1984) 715–720, http://dx.doi.org/10.1111/j.1151-2916.1984.tb19507.x.

[27] J. Hu, H. Xiao, P. Gao, et al., Synthesis of SiC–TiC composite powders by carbothermal reduction and their sintering behavior, J. Ceram. Process. Res. 14 (1) (2013) 77–81.

[28] Z. Zhou, D. Xia, Z. Li, et al., Preparation of ZrB_2–SiC–LaB_6 ultrafine multiphase powders by sol–gel and carbothermal/borothermal reduction, Mater. Sci. Eng. Powder Metall. 28 (03) (2023) 223–232, http://dx.doi.org/10.19976/j.cnki.43-1448/TF.2023005.

[29] J. Liu, L. Xu, W. Yue, et al., Preparation of β-SiAlON/SiC composite ceramic foam filters and their oxidation resistance, Ceram. Int. 50 (20PA) (2024) 38200–38208, http://dx.doi.org/10.1016/J.CERAMINT.2024.07.183.

[30] Z. Hong, Q. Zhang, K. Li, et al., Oxidation behavior of SiC/SiC composites in air at high temperature, J. Mater. Eng. 49 (5) (2021) 144–150, http://dx.doi.org/10.11868/j.issn.1001-4381.2020.001169.

[31] T. Tian, W. Sun, X. Xiong, et al., Effect of VC content on the microstructure, ablation and oxidation resistance of the protective oxide layer of C/C-ZrC-VC-SiC composites, Corros. Sci. 237 (2024), http://dx.doi.org/10.1016/J.CORSCI.2024.112327, 112327.

[32] Y. Zhang, J. Zhang, Z. Fu, et al., Oxidation resistance analysis of zirconium carbide sintered by hot-pressing, J. Chin. Ceram. Soc. 41 (7) (2013) 901–904, http://dx.doi.org/10.7521/j.issn.0454-5648.2013.07.05.